

Sensitive absorption spectroscopy with a room-temperature distributed-feedback quantum-cascade laser

K. Namjou, S. Cai, and E. A. Whittaker

Department of Physics and Engineering Physics, Stevens Institute of Technology, Hoboken, New Jersey 07030

J. Faist, C. Gmachl, F. Capasso, D. L. Sivco, and A. Y. Cho

Bell Laboratories, Lucent Technologies, 700 Mountain Avenue, Murray Hill, New Jersey 07974

Received September 18, 1997

We report what we believe are the first spectroscopic measurements to be made with a room-temperature quantum-cascade distributed-feedback laser. Using wavelength modulation spectroscopy, we detected N_2O and CH_4 in the chemical fingerprint wavelength range near $8\ \mu m$. The noise equivalent absorbance for our measurement was 5 parts in 10^5 , limited by excess amplitude modulation on the laser output, which corresponds to a 1-Hz bandwidth detection limit of 250 parts N_2O in 10^9 parts N_2 in a 1-m path length. © 1998 Optical Society of America

OCIS codes: 140.5960, 300.1030, 300.6340, 280.3420.

There is a wide range of measurement and control applications that require, *in situ*, chemically selective detection of molecular species in the gas phase. Laser absorption spectroscopy is ideally suited for this purpose, and low detection limits have been reported.^{1–3} Because the strongest line strengths for molecules occur in the middle-infrared portion of the spectrum, the lead salt family of tunable semiconductor diode lasers has been the standard choice for use in this spectral region. Effective methods for detecting weak absorbances have been developed.^{3,4} However, as a source in a practical sensing instrument these devices have two limitations: Lead salt lasers must always be operated cryogenically, and they are available commercially only as Fabry–Perot cavity oscillators and hence are subject to cavity mode hopping and tuning gaps.

The quantum-cascade (QC) laser^{5–8} overcomes these two drawbacks, and we report here what is to our knowledge the first application of the QC laser to the detection of dilute samples of molecules through their absorption spectrum. The QC laser derives its gain from the transition of electrons between two excited states in the conduction band of a coupled quantum-well structure. Inversion is obtained by careful engineering of the carrier lifetimes, determined by longitudinal phonon scattering. The active region and a matching electron injector are cascaded many times to increase output power. The lasing wavelength is determined by the thickness of the active region's quantum-well layer, essentially independently of the semiconductor bandgap. Devices with wavelengths ranging from 4 to $11\ \mu m$ have been fabricated with an AlInAs/InGaAs lattice matched to InP.⁷ This spectral range overlaps the most important part of the molecular fingerprint region and includes a substantial fraction of the lead salt lasing range. However, unlike the lead salt laser, the QC laser is capable of operating at room temperature and above.⁹ Furthermore, room-temperature QC lasers with a distributed-feedback (DFB) architecture have also

been demonstrated to have continuous, single-mode tuning of $>20\ cm^{-1}$.¹⁰

Figure 1 diagrams a sensitive detection measurement that we implemented by using such a QC DFB laser. The laser, designed to emit near $8\ \mu m$,¹⁰ is mounted in a temperature controlled, evacuated chamber. The laser is driven by a 2.6-A amplitude, 1-MHz train of 11-ns-wide current pulses ($\sim 1\%$ duty factor), resulting in $10\text{-}\mu W$ collected average laser output power. The thermoelectric cooler temperature is set to $4\ ^\circ C$. This setup tunes the laser resonance close to the N_2O absorption line of interest. We fine tune the laser by superimposing upon the pulsed waveform a 4-Hz current ramp, which alone would be insufficient in amplitude to bring the laser above threshold but which causes a temperature modulation on the laser sufficient to sweep the lasing frequency by approximately one wave number. Finally, we combine the ramp with a 1.8-kHz sinusoidal dither, which adds a second, higher-frequency temperature modulation, resulting in a concomitant wavelength modulation (WM).¹¹

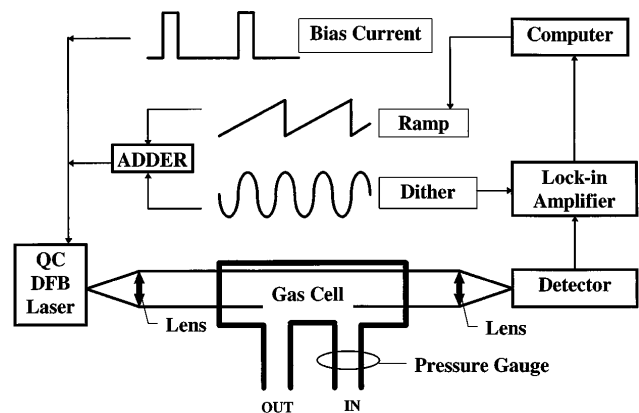


Fig. 1. Experimental arrangement for wavelength modulation spectroscopy with the quantum-cascade DFB laser.

The modulated laser beam is collimated and then directed through a 10-cm-long gas cell equipped with wedged CaF_2 windows. The transmitted light is focused onto a HgCdTe photoconductive detector, cooled to 77 K. The detector is coupled to a matched preamplifier whose output is detected by a lock-in amplifier. The wavelength-modulation dither serves as the lock-in reference, and the lock-in output is recorded with a 14-bit digital signal-processor-equipped computer. The computer records individual ramp scans and can be set to average these scans. The data reported here were recorded mostly by use of 16-scan averaging with a lock-in bandwidth of 250 Hz, resulting in a net detection bandwidth of 16 Hz. Because the dither frequency is much lower than the underlying pulse repetition frequency, this arrangement results in WM absorption spectroscopy.

The gas cell was filled with commercially premixed volumes of diluted gas, which were further diluted with high-purity dry N_2 . For most of the measurements reported here we used samples of 10%, 1%, and 0.1% N_2O in N_2 diluted in steps of five as many as three times with total pressures from 1 to 20 Torr.

By fixing the temperature of the thermoelectrically cooled laser head, we obtained sets of scans by using the 4-Hz current ramp, whose center frequency could be estimated from the wavelength calibration of the QC DFB laser obtained independently with a Fourier-transform infrared spectrometer.¹⁰ Figure 2 shows several such scans overlaid to provide a continuous temperature scan from $\sim -17^\circ\text{C}$ to 6°C , corresponding to a 2.5-cm^{-1} laser frequency scan starting at 1280 cm^{-1} . The spectral data show the characteristic derivative line shape of WM spectroscopy obtained from a 10% $\text{N}_2\text{O}/90\%$ N_2 premixed sample with a total pressure of 1 Torr. We checked the frequency calibration by comparing the data with the known frequencies and line strengths of the N_2O $10^0\text{-}00^0$ band obtained from the HITRAN database.¹² These are shown on the bottom of the figure. As an additional check on frequency calibration we include a scan obtained from a 10% $\text{CH}_4/90\%$ N_2 sample at 10-Torr total pressure.

By switching the laser modulation from frequency dither to mechanical chopping we were able to measure direct absorption and thus calibrate the WM signal to absolute absorbance. Figure 3(a) shows the resultant spectral scans obtained with 40 Torr of the 10,000-parts-in- 10^6 (ppm; 1%) N_2O -in- N_2 sample. The solid curve shows the absorption dip associated with one of the strong N_2O lines from Fig. 2. The dotted curve shows a background trace with the gas cell evacuated, and the dashed-dotted curve shows the trace with the beam blocked. We obtained the dashed trace by passing the beam through a 1.44-GHz free-spectral-range solid germanium etalon.

Figure 3(b) shows the fractional attenuation of the laser beam on line center as a function of N_2O concentration inferred from the magnitude of the absorption dip for the 10,000-ppm sample and two $5\times$ dilution steps (circles) and the undiluted 1000-ppm sample (square). The straight line is a least-squares fit to the data including the point (0 absorbance, 0 ppm). The slight deviation at low concentration is due

to accumulated error in dilution and the low signal-to-noise ratio at low absorbance.

WM affords a substantial improvement over the direct measurement in sensitivity to absorbance. Using the two premixed samples of N_2O and the dilution procedure outlined above, we measured the WM signal amplitude for one of the strongest N_2O lines as a function of N_2O concentration. We calibrated the WM signal for absorbance by matching the WM signal to the directly measured absorbance at the highest concentrations. The result is plotted in Fig. 4. The solid line is a linear least-squares fit from the data from dilutions of both premixed samples, where we forced the

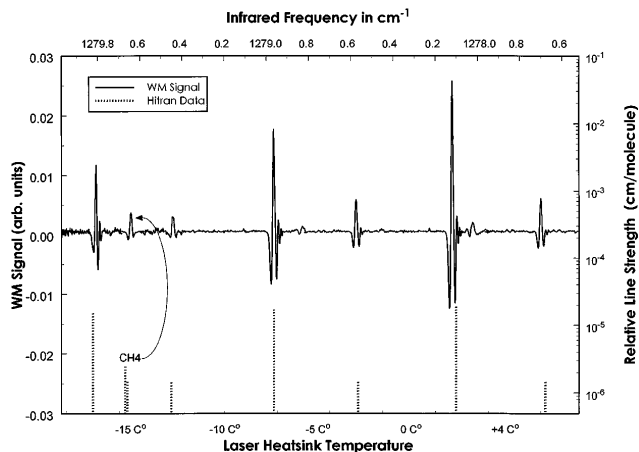


Fig. 2. WM signal versus laser frequency for 10% diluted samples of N_2O and CH_4 with corresponding HITRAN data plotted below.

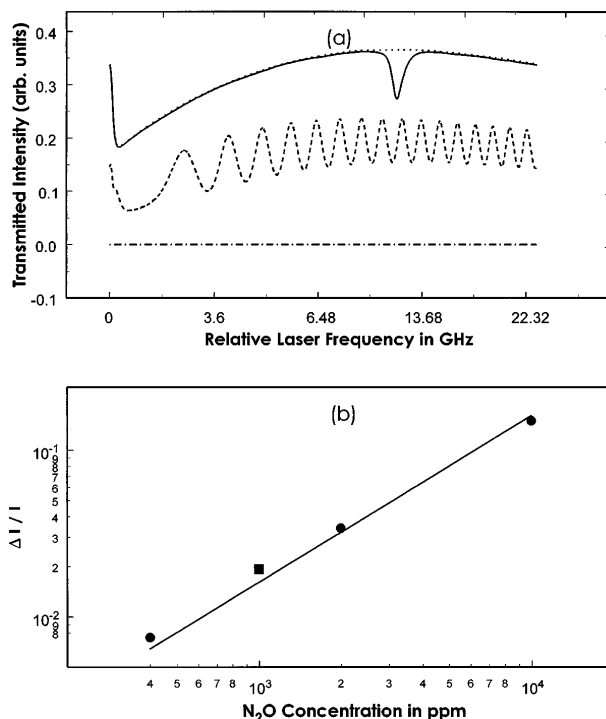


Fig. 3. (a) Transmitted laser power versus frequency with the N_2O sample (solid curve), a calibration etalon (dashed curve), or an opaque block (dotted-dashed line) in the beam. (b) Absorbance versus concentration, obtained by dilution of the samples as discussed in the text.

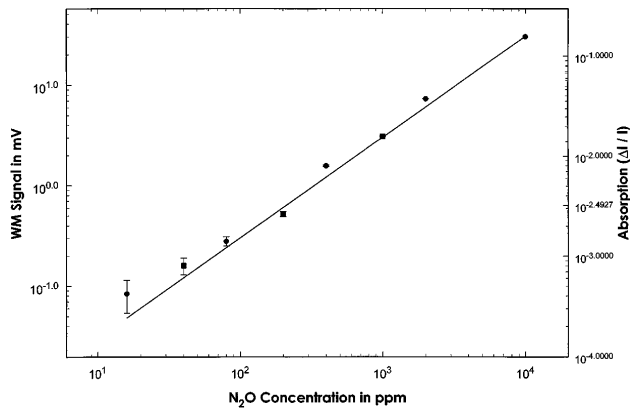


Fig. 4. Plot of WM signal amplitude versus N_2O concentration for 20-Torr total pressure samples. The error bars represent the amplitude of the background signal fluctuations depicted in Fig. 5.

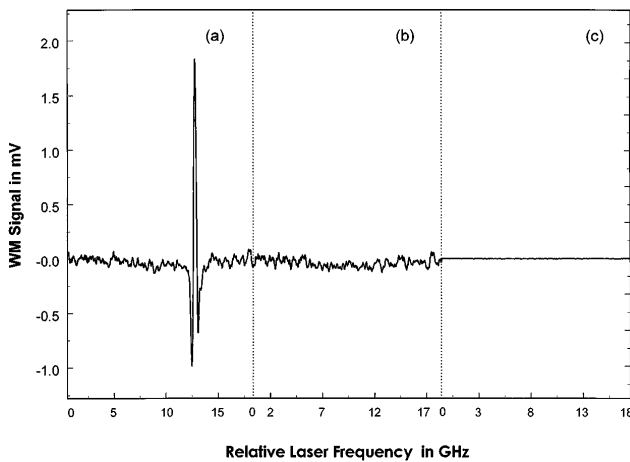


Fig. 5. (a) WM signal that is due to a 1000-ppm N_2O sample at 10-Torr total pressure. (b) Background trace for an evacuated sample cell. (c) Background trace with the laser beam blocked.

fit to pass through point (0, 0) as before. Below a dilution of 20 ppm we were unable to distinguish the WM signal from background fluctuations, which are indicated by the error bars on the figure. To estimate the noise equivalent absorbance we show in Fig. 5(a) the WM signal from the 1000-ppm sample at 10 Torr and in Fig. 5(b) the trace obtained with the gas cell evacuated to less than 10 mTorr. The rms amplitude of the random component of the signal was found to be approximately $10 \mu\text{V}/\sqrt{\text{Hz}}$. Comparing this signal level with the absorbance sensitivity deduced from Fig. 4, we estimate the noise equivalent absorbance to be $5 \times 10^{-5}/\sqrt{\text{Hz}}$. With the strongest N_2O line in this spectral region, this absorbance corresponds to a detection limit of $\sim 0.25 \text{ ppm}\cdot\text{m}/\sqrt{\text{Hz}}$.

We show in Fig. 5(c) the background obtained with the laser beam blocked. The $280\text{-nV}/\sqrt{\text{Hz}}$ amplitude is consistent with that expected from 300-K background radiation. We conclude that the limiting background of our measurement is due to excess amplitude modulation that appears on the output of the laser.

In conclusion, we have demonstrated sensitive detection of dilute samples of N_2O , using a quantum-cascade

DFB laser operated near 4°C . The noise equivalent absorbance of $5 \times 10^{-5}/\sqrt{\text{Hz}}$ is limited by two nonfundamental factors. Sensitivity to absorbance is reduced because of excess laser line broadening.¹¹ The apparent laser linewidth of 720 MHz is due to the frequency chirp that results from the pulsed operation and the heating during the current pulse. This is in strong contrast to the linewidth observed for continuous wave operation.¹³ Furthermore, amplitude noise from the drive electronics imparts an additional background at the dither frequency. A factor-of-3–5 improvement in both factors should be possible with improved device characteristics and optimized drive electronics. Combined with the use of high-frequency-modulation techniques, these improvements should bring the sensitivity of the QC DFB laser to within an order of magnitude of the $6 \times 10^{-8}/\sqrt{\text{Hz}}$ minimum detectable absorbance reported for frequency-modulated lead salt lasers.¹⁴ We conclude that, combined with the advantage of room-temperature laser operation, the detection sensitivity demonstrated here will make the QC DFB laser an excellent choice for sensitive absorption spectroscopy detection of species with strong vibrational features in the chemical fingerprint spectral region.

We acknowledge partial support from the Defense Advanced Research Projects Agency and the U.S. Army Research Office under contract DAAH04-96-C-0026 (Bell Labs) and the National Science Foundation (Stevens Institute) under grant DMI-9313320.

References

1. J. A. Silver, *Appl. Opt.* **6**, 707 (1992).
2. C. B. Carlisle and D. E. Cooper, *Appl. Phys. Lett.* **56**, 805 (1990).
3. P. Werle, *Appl. Phys. B* **60**, 499 (1995).
4. H. C. Sun and E. A. Whittaker, *Appl. Phys. Lett.* **63**, 1035 (1993).
5. J. Faist, F. Capasso, D. L. Sivco, C. Sirtori, A. L. Hutchinson, and A. Y. Cho, *Science* **264**, 553 (1994).
6. J. Faist, F. Capasso, D. L. Sivco, A. L. Hutchinson, C. Sirtori, and A. Y. Cho, *Appl. Phys. Lett.* **65**, 2901 (1994).
7. F. Capasso, J. Faist, C. Sirtori, and A. Y. Cho, *Solid State Commun.* **102**, 231 (1997).
8. J. Faist, F. Capasso, C. Sirtori, D. L. Sivco, J. N. Baillargeon, A. L. Hutchinson, S. N. G. Chu, and A. Y. Cho, *Appl. Phys. Lett.* **68**, 3680 (1996).
9. C. Sirtori, J. Faist, F. Capasso, D. L. Sivco, A. L. Hutchinson, and A. Y. Cho, *IEEE Photon. Technol. Lett.* **9**, 294 (1997).
10. J. Faist, C. Gmachl, F. Capasso, C. Sirtori, D. L. Sivco, J. N. Baillargeon, and A. Y. Cho, *Appl. Phys. Lett.* **70**, 2670 (1997).
11. J. M. Supplee, E. A. Whittaker, and W. Lenth, *Appl. Opt.* **33**, 6294 (1994).
12. L. S. Rothman, R. R. Gamache, A. Goldman, L. R. Brown, R. A. Toth, H. M. Pickett, R. L. Poynter, J. M. Flaud, C. Camy-Peyret, A. Barbe, N. Husson, C. P. Rinsland, and M. A. H. Smith, *Appl. Opt.* **26**, 4058 (1997).
13. F. Capasso, D. L. Sivco, A. L. Hutchinson, and A. Y. Cho, *Appl. Phys. Lett.* **67**, 3057 (1995).
14. P. Werle, F. Slemr, M. Gehrtz, and C. Bräuchle, *Appl. Phys. B* **49**, 99 (1989).